

A phase conjugate mirror inspired approach for building cloaking structures with left-handed materials

Guoan Zheng^{1,3}, Xin Heng² and Changhui Yang¹

¹ Electrical Engineering, California Institute of Technology, Pasadena, CA 91125, USA

² Rowland Institute at Harvard, Harvard University, Cambridge, MA 02142, USA

E-mail: gazheng@caltech.edu

New Journal of Physics **11** (2009) 033010 (15pp)

Received 10 November 2008

Published 4 March 2009

Online at <http://www.njp.org/>

doi:10.1088/1367-2630/11/3/033010

Abstract. In this paper, we propose and examine a new cloaking method, which was inspired by the close correspondence between a phase conjugate mirror and the interface between a pair of matched right-handed material (RHM) and left-handed material (LHM) media. Using this method, we show that a symmetric conducting shell embedded in the interface junction of an isotropic RHM layer and an isotropic negative index or LHM layer can serve as a limited cloaking structure. The proposed structure presents an anomalously small scattering cross-section to an incident propagating electromagnetic (EM) field. The interior of the shell can be used to shield small objects from interrogation. We report the results of 2D finite-element-method (FEM) simulations that were performed to verify the principle, and discuss the limitations of the proposed structure.

³ Author to whom any correspondence should be addressed.

Contents

1. Introduction	2
2. A matched RHM–LHM structure for cloaking a known lossless scattering object	3
2.1. Principle	3
2.2. Simulation of the matched RHM–LHM cloaking structure	7
2.3. Ancillary result: an EM tunnel based on the RHM–LHM structure	9
3. An RHM–PEC–LHM cloaking structure	9
3.1. Principle	9
3.2. Simulation of the RHM–PEC–LHM cloaking structure	11
4. Conclusion	15
Acknowledgment	15
References	15

1. Introduction

Phase conjugation is an interesting wave phenomenon in which both the direction of propagation and the overall phase factor for each arbitrary plane-wave component are precisely reversed during reflection from a phase conjugate mirror (PCM) [1, 2]. Thus if someone is mirrored by a PCM, he/she will see nothing but his/her own pupils, or to be more specific, he/she will see his/her left pupil with his/her left eye and he/she will see his/her right pupil with his/her right eye. One of the remarkable properties of PCMs is the anti-scattering effect, i.e. the backscattering wave of the lossless scatterers can be canceled and the distortion of the wave field introduced by the scatterers can be corrected. This anti-scattering property of PCMs has been extensively studied before (see for example [1]–[4]). Based on such an effect, PCMs have found a lot of applications in, for example, compensating for optical signal distortions [1, 2], suppressing the turbidity of biological tissue [5], enhancing near-field light components [6, 7], and constructing novel interferometers and resonators [1, 8]. Despite the broad range of uses that a PCM can be employed in, implementing a true PCM experimentally remains a tough challenge. Holography methods [9] provide static solutions but are not suited for addressing situations with time-varying components. Real-time approaches, such as four-wave mixing, can respond to changes in time but the effective reflectivity of such approaches is generally much less than unity [1].

Recently, we showed that the interface between a matched positive index material (or right-handed material (RHM)) and a negative index material (or left-handed material (LHM)) interacts with propagative electromagnetic (EM) fields in ways that are very similar to a PCM [10]. This prompts us to explore the possibility of duplicating the anti-scattering characteristics of the PCM with novel and useful RHM–LHM structures. We recognize that approaches for implementing LHM are only in their early stages of development, but we are optimistic that LHM technology will rapidly mature in the near future.

In this paper, we present two proposed novel structures. The first structure uses the direct correspondence between a PCM and a RHM–LHM interface to translate the anti-scattering property of a PCM to create a RHM–LHM structure that is capable of cloaking a known lossless scattering object. We show that, in both theory and simulation, such a structure is transparent to an incident EM field. As an ancillary result, we also show that this structure can be adopted

to spatially transport an EM field without significant wavefront distortion. The second proposed structure is aimed at cloaking an object without knowledge of its properties by encasing it within a perfect electric conductor (PEC) shell. We show that by embedding such a shell within a matched pair of RHM and LHM layers, the shell can present an anomalously small scattering cross-section.

We note that several methods for achieving an invisibility cloak have been reported over the past few years [11]–[19]. One prominent method relies on a coordinate transform, i.e. an optical conformal mapping method where empty space is transformed into a shell surrounding the object to be concealed [11]–[14]. The key implementation challenge for such a design lies in the strong anisotropy of the material and the complicated position-dependent function with which the EM parameters are associated [11].

The cloaking structure proposed here is limited in its cloaking ability in comparison to structures based on conformal mapping. However, the structure proposed here is comparatively conceptually simple and it illustrates a previously unreported way for tackling the cloaking challenge by drawing correspondence from PCMs.

2. A matched RHM–LHM structure for cloaking a known lossless scattering object

2.1. Principle

The operating principle of the matched RHM–LHM structure is best explained by describing the two concepts that underpin it. *Concept 1*: the placement of a PCM behind a lossless scattering object in a bounded waveguide will lead to the cancelation of its backscattered light field components. *Concept 2*: the interaction of a light field and scatterers with a PCM can be modeled by substituting the PCM with a RHM–LHM interface and associated image sources and objects in the LHM. This equivalency is valid for propagative wave components.

Concept 1 was described and proven in [3]. For completeness, we present a short version of the proof here.

Consider the following structure (figure 1(a)). In this scenario, an incident wave (denoted by the black arrow) impinges on a lossless scatterer with arbitrary shape in front of a PCM. As with the proof given in [3], we impose the condition that the scatterer is placed within a bounded waveguide in which the top and bottom faces are PEC. (Note that the anti-scattering phenomenon in concept 1 extends to a scatterer placed in open space as well. The proof can be found in [3], but that result is not useful for us in this present study.) In order to prove concept 1, we introduce the scattering matrix S , which relates the incident and reflected fields at the terminal ports of the waveguide (figure 1(b)):

$$\begin{pmatrix} b_1 \\ b_2 \end{pmatrix} = \begin{pmatrix} S_{11} & S_{12} \\ S_{21} & S_{22} \end{pmatrix} \begin{pmatrix} a_1 \\ a_2 \end{pmatrix}. \quad (1)$$

Since the structure discussed here is assumed to be lossless and reciprocal, the scattering matrix should be unitary and symmetric [4, 20]. Explicitly, we have

$$S_{11}S_{12}^* + S_{12}S_{22}^* = 0, \quad S_{21}S_{12}^* + S_{22}S_{22}^* = 1, \quad S_{11}S_{11}^* + S_{12}S_{21}^* = 1, \quad (2a)$$

$$S_{12} = S_{21}, \quad (2b)$$

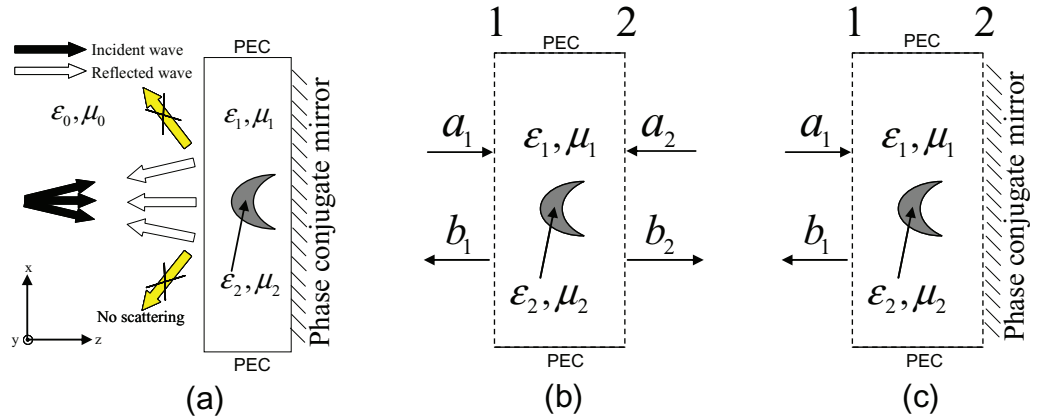


Figure 1. (a) The distortion–correction effect of the PCM. All the reflected wave will retrace its path back to the source, and there is no scattering wave going in other directions. (b) A two-port system showing the incident and scattering fields. (c) A one-port system backed by the PCM.

where ‘*’ denotes the complex conjugate. Now we introduce a PCM at port 2 (see figure 1(c)). The function of the PCM is to reflect the incident field by conjugating its phase. Let a_1 be the incident field at port 1 (figure 1(c)). The field reflected by the lossless scatterer back to port 1 is given by $S_{11}a_1$. The transmitted field component, $S_{21}a_1$, that would have exited via port 2 is instead reflected by the PCM and can be expressed by $S_{21}^*a_1^*$. The field component will interact again with the scatterer. A portion of it, given by $S_{22}S_{21}^*a_1^*$, is reflected back to the PCM. At the same time, a field $S_{12}S_{21}^*a_1^*$ is transmitted to port 1. The multiple scattering between the PCM and scatterer continues on *ad infinitum*, and, each time, this process contributes an additional term to the field at port 1. Using the relation in equation (2), the total wave field b_1 reflected at port 1 is

$$\begin{aligned}
 b_1 &= S_{11}a_1 + S_{12}S_{21}^*(1 + S_{22}^*S_{22} + \dots)a_1^* + S_{22}^*S_{21}S_{12}(1 + S_{22}S_{22}^* + \dots)a_1 \\
 &= \left(S_{11} + \frac{S_{12}S_{22}^*S_{12}}{1 - S_{22}S_{22}^*} \right) a_1 + \left(\frac{S_{12}S_{21}^*}{1 - S_{22}^*S_{22}} \right) a_1^* = a_1^*.
 \end{aligned} \tag{3}$$

Thus we have shown that the introduction of the PCM at port 2 effectively cancels out the backscattered field $S_{11}a_1$ completely and replaces it with a_1^* , traveling in the direction opposite to the incident field.

Concept 2 was first described and proven in [10]. An illustration that outlines this equivalency is shown in figures 2(a) and (b). The concept is best appreciated by drawing parallels to the concept that the electric-field contribution of a charge distribution at a distance from a grounded conductive interface is identical to the distribution associated with the scenario where the conductive interface is replaced by a virtual and oppositely charged charge distribution at the same distance behind the interface—the ‘ghost charge’ model. The ‘ghost charge’ model provides an excellent means for solving electric-field distribution problems because it automatically accounts for the zero-transverse-electric-field boundary condition at the interface. Likewise, the replacement of the PCM with a RHM–LHM interface and associated image sources and objects in the LHM automatically accounts for the zero-imaginary

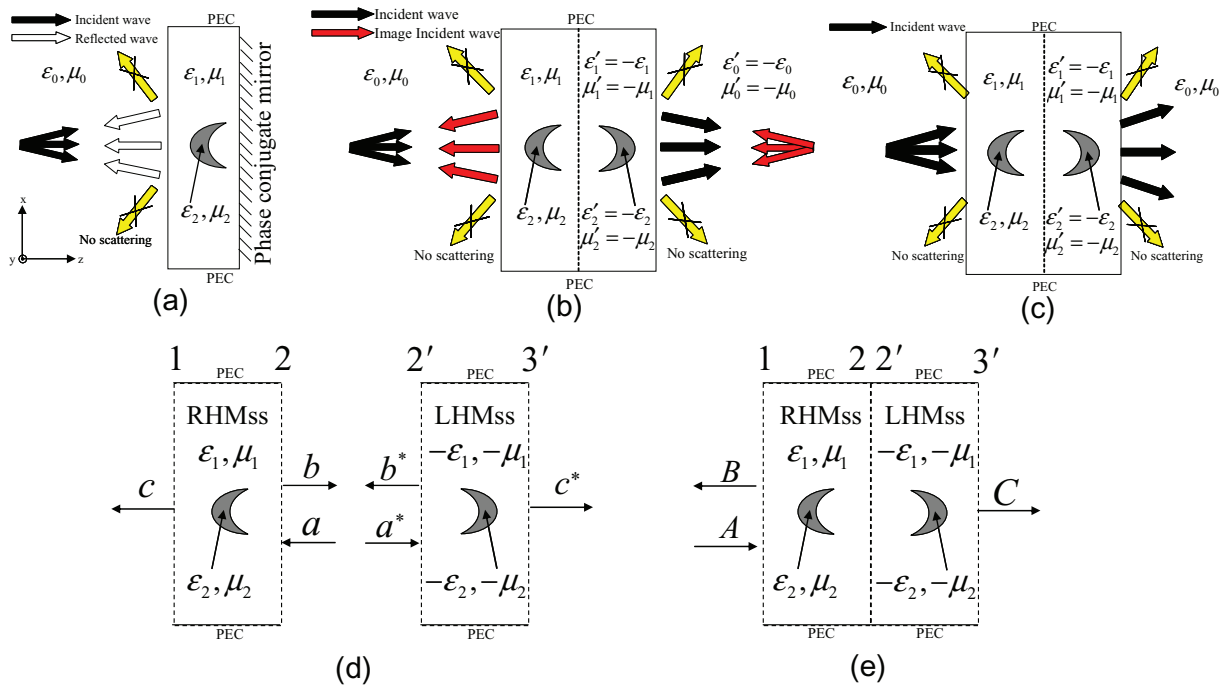


Figure 2. (a) The distortion–correction effect of PCM. (b) The equivalent model for PCM utilizing the RHM–LHM interface. (c) The proposed cloaking structure. (d) The RHM and LHM sub-structure. (e) The proposed cloaking structure, which is a combination of two sub-structures.

component of the electric field at the interface. We note that this equivalency of a PCM with RHM–LHM is strictly valid for propagative wave components and is not valid for evanescent wave components; however, this point has little relevance as long as the propagative wave components at the interface dominate over the evanescent wave components.

Applying the idea of concept 1, we can see that the structure shown in figure 2(a) will reflect the light towards its source and no backscattered light components should exist. Despite the fact that the structure in figure 2(a) possesses anti-scattering properties, it is not a cloaking device as it does not allow an incident EM field to freely propagate through it.

We need to take two steps to change the structure in figure 2(a) into an appropriate cloaking structure, as illustrated in figures 2(b) and (c), respectively. Firstly, by exploiting concept 2, we replace the PCM with an LHM (with negative permittivity and permeability) and an appropriately altered duplicate of the space before the PCM interface [10], as shown in figure 2(b). We note that the equivalency of these two models implies the absence of spurious scattered waves in both figures 2(a) and (b). Secondly, we remove the image source in figure 2(b) and make $\epsilon'_0 = \epsilon_0, \mu'_0 = \mu_0$, as shown in figure 2(c). This allows us to accomplish two things. Firstly, the removal of the artificial image source allows us to remove the unwanted phase-conjugated wave that travels back to the original source. Secondly, by setting $\epsilon'_0 = \epsilon_0, \mu'_0 = \mu_0$, it frees us from having to fill the entire right half of the plane with LHM medium. We note that this change does not alter the reflection and transmission coefficients of fields interacting with the structure's interface in figure 2(c). Specifically, the reflection coefficient of any given TM field (the transmission coefficient and the case of TE field can be treated in the same manner) of

media A and B is given by $R_{AB} = (k_{pA}/\varepsilon_A - k_{pB}/\varepsilon_B)/(k_{pA}/\varepsilon_A + k_{pB}/\varepsilon_B)$, where k_{pA} and k_{pB} are the wave vectors in media A and B that are perpendicular to the interface. For the propagating field, a sign flip of the permittivity (ε_B) and permeability (μ_B) of medium B results in a sign flip of k_{pB} and ε_B in the equation of R_{AB} [10, 21], and thus, the reflectivity coefficient R_{AB} does not change for the propagating field. Therefore, in figure 2(c), when we change the permittivity $-\varepsilon_0$ and permeability $-\mu_0$ of a material to ε_0 and μ_0 , the reflection and transmission coefficients do not change for the propagating field. In other words, setting $\varepsilon'_0 = \varepsilon_0$, $\mu'_0 = \mu_0$ in figure 2(c) does not change the impedance relation of the structure, and we do not expect any spurious scattered wave in the right half of the structure in figure 2(c).

The structure shown in figure 2(c) comprises our first invisibility cloak structure. For any given lossless scatterer that we would like to conceal, we would need to make a left-handed duplicate of the scatterer and put the scatterer and its left-handed duplicate symmetrically about the RHM–LHM interface. The entire structure should freely permit EM field to propagate through it without significant angular deflections.

The cloaking property of the proposed structure can be formally explained through a scattering-matrix model. This approach is independent of the spatial dimension of the problem (i.e. the result is valid both for 2D and 3D), and it is independent of the size of the lossless scatterer. We divide figure 2(c) into two sub-structures shown in figure 2(d): one is the RHM sub-structure (RHMss) and the other is the LHM sub-structure (LHMss). The scattering matrixes for these two sub-structures can be expressed as

$$S = \begin{pmatrix} S_{11} & S_{12} \\ S_{21} & S_{22} \end{pmatrix}, \quad S' = \begin{pmatrix} S'_{22} & S'_{23} \\ S'_{32} & S'_{33} \end{pmatrix}, \quad (4)$$

where S is for the RHMss and S' is for the LHMss.

We can gain insights into the relationship of these two matrices by considering the following scenario (figure 2(d)). Consider a situation where an incident wave (denoted by ‘a’) impinges the right face (port 2) of the RHMss, the reflected wave (denoted by ‘b’) and the transmitted wave (denoted by ‘c’) can be expressed as

$$b = S_{22}a, \quad c = S_{12}a. \quad (5)$$

The same argument can be applied to the LHMss, thus

$$b' = S'_{22}a', \quad c' = S'_{32}a'. \quad (6)$$

It has been shown that the time-dependent field expressions in the LHMss differ from the RHMss only by complex conjugation [22]. Therefore, in the LHMss, if $a' = a^*$, we can get $b' = b^*$ and $c' = c^*$ in equation (6), where ‘*’ stands for the complex conjugate. And thus

$$S'_{22} = S_{22}^*, \quad S'_{32} = S_{12}^*, \quad (7)$$

which are important relations of the two sub-structures. Since the sub-structures discussed here are assumed to be lossless and reciprocal, the scattering matrix should be unitary and symmetric [4, 20]. Explicitly, we have

$$S_{11}S_{12}^* + S_{12}S_{22}^* = 0, \quad S_{21}S_{12}^* + S_{22}S_{22}^* = 1, \quad (8a)$$

$$S_{12} = S_{21}. \quad (8b)$$

Combining the two sub-structures, we get the proposed cloaking structure in figure 2(e). Assuming the incident, reflected and transmitted wave are ‘A’, ‘B’ and ‘C’ in this case, we can get the relations between these three waves by considering the multiple scattering process, with the result:

$$\begin{aligned} B &= S_{11}A + S_{12}S'_{22}S_{21}A + S_{12}(S'_{22}S_{22})S'_{22}S_{21}A + S_{12}(S'_{22}S_{22})^2S'_{22}S_{21}A + \dots \\ &= S_{11}A + S_{12}S'_{22}S_{21}A \left(\frac{1}{1 - S'_{22}S_{22}} \right), \end{aligned} \quad (9a)$$

$$C = S'_{32}S_{21}A + S'_{32}(S'_{22}S_{22})S_{21}A + S'_{32}(S'_{22}S_{22})^2S_{21}A + \dots = \left(\frac{S'_{32}S_{21}A}{1 - S'_{22}S_{22}} \right), \quad (9b)$$

where $S_{11}A$ in equation (9a) is the singly reflected wave from the RHMss, $S_{12}S'_{22}S_{21}A$ is the wave that transmitted through the RHMss ($S_{21}A$) and then was reflected by the LHMss ($S'_{22}S_{21}A$) and finally returned to the left face of the RHM slab or port 1 ($S_{12}S'_{22}S_{21}A$). The multiple scattering between the RHMss and LHMss continues on *ad infinitum*. Each time, this process contributes an additional term to the field at port 1 in equation (9a). Equation (9b) can be explained in the same manner. Using equations (7) and (8) to simplify equation (9), we find a surprisingly simple result:

$$B = 0, \quad C = A. \quad (10)$$

Equation (10) has several significant implications. (i) The incident waves should totally transmit through the cloaking structure, and thus the lossless scatterer, together with its left-handed duplicate cannot be ‘seen’ by an outside observer. (ii) There is no phase retardation between the incident and transmitted wave. In other words, the wave emerging at port 3' is the same as the wave entering port 1. Therefore, the observer will see a shifted image of the illumination source, with the shifted distance equal to the width of the cloaking structure. This point is best appreciated by noting that light transmissions through it accrue no optical delays.

2.2. Simulation of the matched RHM–LHM cloaking structure

In order to demonstrate the limited-cloaking property of the proposed structure, we performed a set of simulations using a commercial finite-element-method (FEM) program, COMSOL Multiphysics [23]. The simulations are in 2D and in TM mode. Figure 3 shows the resulting simulated magnetic-field distribution (H_y) and EM power-flow lines for five cases. We impose a small loss term (0.01i) on the LHM to avoid the infinite resonance of the EM field at the interface of RHM and LHM; this consideration was explained in detail in [10].

Displayed in each sub-figure is the real part of the magnetic-field phasor at 1 GHz (equivalent to the time-domain fields at the instant of time when the source phase is zero) so that the individual phase fronts are clearly visible. The direction of the power-flow lines (denoted as the black lines) is the direction of the Poynting vector and the line density is proportional to the magnitude of the magnetic field. In figures 3(a)–(c), a plane wave at normal incidence is considered. In figures 3(d) and (e), an infinitesimally thin line source is used to generate a cylindrical wave. By comparing the scenarios where the cloaking structures are present (figures 3(a) and (d)) to those where they are absent (figures 3(b) and (e)), the ability of the cloaking structure to deflect the incident field minimally can be seen clearly. From figure 3(d),

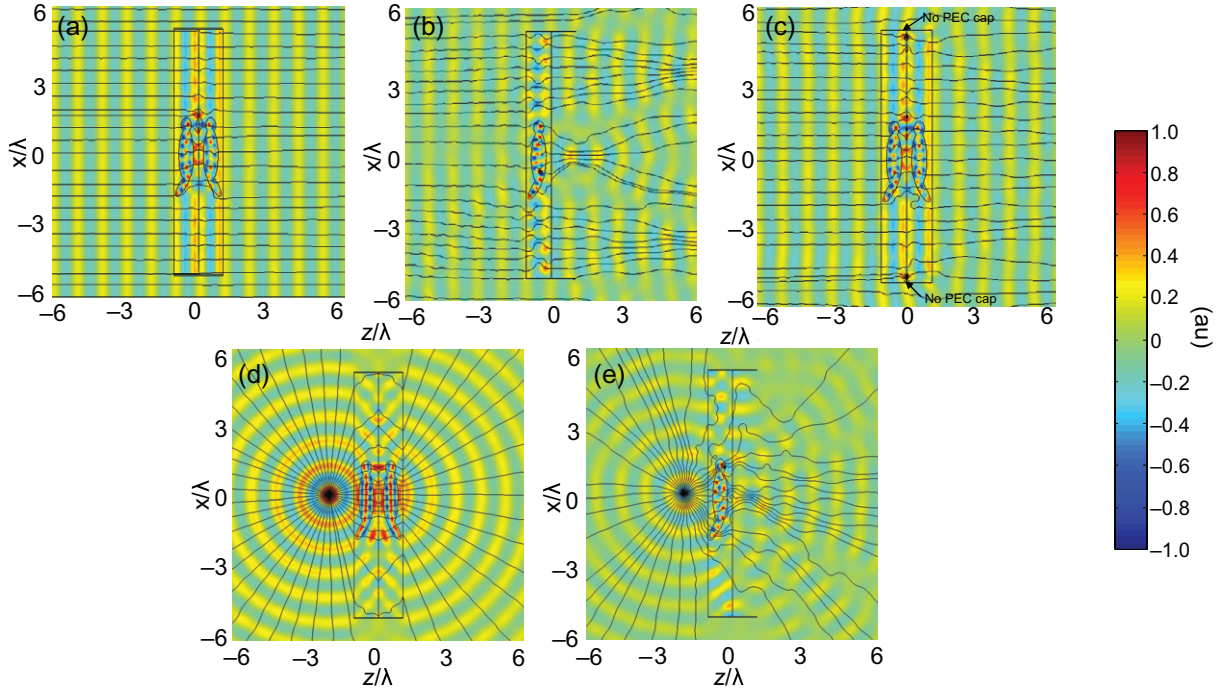


Figure 3. The simulated magnetic-field distribution and EM power-flow lines for the RHM–LHM structure. The computational domain is $3.6 \text{ m} \times 3.6 \text{ m}$ (12 wavelengths), where a 1 GHz transverse-electric TM polarized time-harmonic wave is incident upon a lossless scatterer with $\varepsilon_2 = 9$, $\mu_2 = 1$. The width of the proposed cloaking structure in (a) and (d) is 0.6 m (two wavelengths) and the height is 3 m (ten wavelengths). The permittivity and permeability of the cloaking structure are $\varepsilon_1 = 2$, $\mu_1 = 1$, $\varepsilon'_1 = -2 + 0.01i$, $\mu'_1 = -1 + 0.01i$, $\varepsilon'_2 = -9 + 0.01i$, $\mu'_2 = -1 + 0.01i$, $\varepsilon_0 = \varepsilon'_0 = \mu_0 = \mu'_0 = 1$. As a comparison, (b) and (e) are the cases without the proposed cloaking structure. Figure 3(c) is the simulation of the proposed cloaking structure without PEC caps. For all the simulations, we use a perfect match layer (PML) in the outer boundaries to absorb the EM wave.

we can also see that the cloaking structure also displaces the transmitted light field by an amount equal to its thickness as discussed earlier.

In order to quantify the cloaking performance, we define the cloaking efficiency as the ratio of the total scattered power without the cloaking structure (i.e. without the left-handed duplicate as shown in figure 3(b)) to the total scattered power with the cloaking structure:

$$\text{Cloaking efficiency} = \frac{P_{\text{without_cloak}}^{\text{scattering}}}{P_{\text{with_cloak}}^{\text{scattering}}}. \quad (11)$$

The illumination source used is a TM plane wave at normal incidence, as shown in figures 3(a) and (b). The total scattered power is computed by taking the difference between the simulation solution and a simulation where nothing is present; a similar method was used in [24]. For the structure shown in figures 3(a) and (b), the cloaking efficiency is 218, which means that the scattering power with the proposed structure is 1/218 of the scatterer without the structure.

At this point, it is worth taking a closer look at the significance of the PEC caps in the proposed structure. The PEC caps first appeared in figure 1 and were a consequence of the fact we needed a bounded waveguide for the proof of concept 1 (the scattering-matrix approach is only valid in the context of the bounded waveguide). While they may appear spurious in the proposed cloaking structure, they are actually necessary to preserve symmetry when we transit from the structure in figure 2(a) to the one in figures 2(b) and (c). Figures 3(a) and (c) show the difference in light field pattern in the presence and absence of the PEC caps. In this particular simulation, we find that the cloaking efficiency drops from 218 to 16 when the PEC caps are removed.

Finally, we note that this structure is not a true cloak for a number of reasons. Firstly, unlike Pendry's cloak, this structure is unable to cloak an unknown object. In this respect, it is more similar to the cloaking structure proposed by Alu and Engheta [18], which also requires knowledge of the object's properties. The structure proposed in section 3 aims to overcome this limitation to some extent. The second reason is that this structure would visually resemble a clear block of transparent material. This issue can possibly be resolved by stacking the structure in series with a block of optically dense material. In this way, we can match the net refractive index of the ensemble to the surrounding refractive index and thus allow the transmitted light field to accrue appropriate optical delays. Finally, the third reason is that this structure is visible when viewed directly from the top or bottom of the structure. At present, we have no viable strategy for mitigating this issue.

2.3. Ancillary result: an EM tunnel based on the RHM–LHM structure

As an ancillary result, the principle of the proposed RHM–LHM structure can also be adopted to create an EM wave tunnel. From the derivation of equation (10), we see that if the RHMss and LHMss are perfectly matched to each other and symmetrical about their interface, an incident wave can totally transmit through the structure without angular deflection. Such a property can be adopted to create an EM wave tunnel, which allows an incident EM wave to be effectively transported from one region to another without distortion and reflection.

Figure 4(a) shows a design of the proposed EM tunnel. The RHM ($\epsilon_1 = 2$, $\mu_1 = 1$) and LHM regions ($\epsilon'_1 = -2 + 0.01i$, $\mu'_1 = -1 + 0.01i$) in the tunnel are symmetrical about their interface and confined by PEC. As explained earlier, the loss terms are required to avoid the infinite resonance of the EM field at the interface.

The width of the tunnel in this design is 1λ , but the width can be arbitrarily increased to include a wider incident field acceptance range. From figure 4(a), we can see that the wavefront of a line source can propagate through this tunnel without significant distortion (a small amount of distortion and reflection comes from the small loss term in the LHM region). The case where the LHM is substituted with RHM ($\epsilon_1 = 2$, $\mu_1 = 1$) is shown in figure 4(b) as a comparison.

3. An RHM–PEC–LHM cloaking structure

3.1. Principle

The cloaking structure proposed in the last section requires specific knowledge of the lossless scatterer being concealed. In this section, we will discuss a second cloaking structure based on embedding a PEC shell symmetrically between a matched pair of RHM and LHM slabs.

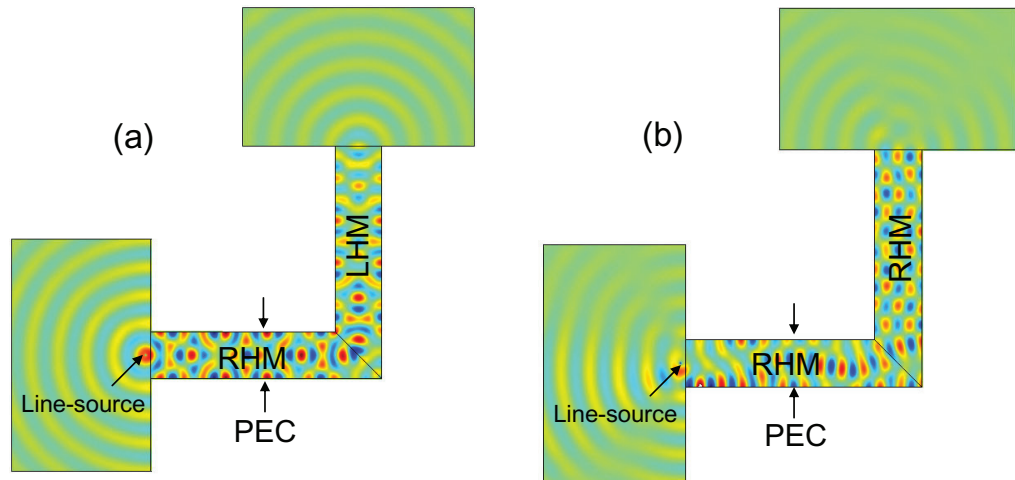


Figure 4. The simulated magnetic-field distribution of the EM tunnel. (a) The EM tunnel that is composed of RHM and LHM, with $\varepsilon_1 = 2$, $\mu_1 = 1$, $\varepsilon_2 = -2 + 0.01i$, $\mu_2 = -1 + 0.01i$. (b) The tunnel which is only composed of RHM, $\varepsilon_1 = 2$, $\mu_1 = 1$.

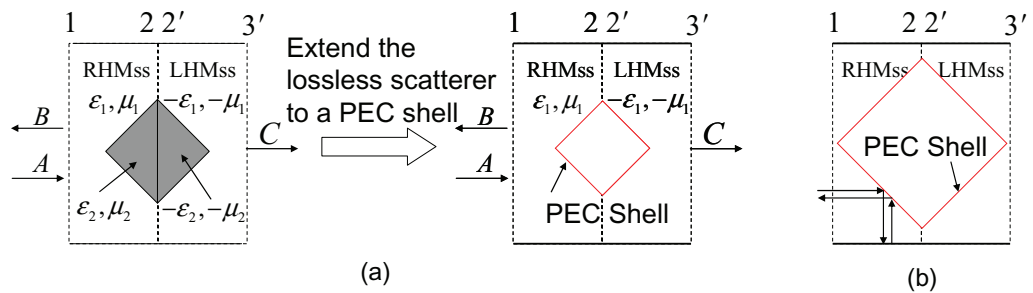


Figure 5. (a) We extend the lossless scatterer to a symmetrical PEC shell. (b) When the shell is large, the light beam (denoted as black arrows) will simply be reflected by the shell and emerges out of port 1 by ray optics considerations.

The interior of the PEC shell can be used to hide an arbitrary object. If we can minimize the scattering profile of the PEC, the structure can potentially function as an effective limited cloak.

In figure 5(a), we show the new RHM–PEC–LHM structure that is derived from the previous RHM–LHM structure. We note that, in the derivation of equation (9), ‘ $|S_{22}| \neq 1$ ’ is assumed (from equation (2), we can see that $|S_{22}| = |S_{11}|$, therefore, $|S_{22}| \neq 1$ also indicates $|S_{11}| \neq 1$); otherwise, the denominator in equation (9) can equal zero and the equation would not be valid. The condition $|S_{22}| = |S_{11}| \neq 1$ is valid for the lossless scatterer in the previous structure, but is invalid for the PEC shell in our present structure. The incident waves associated with $|S_{22}| = |S_{11}| = 1$ are waves that would be scattered by the PEC shell without having an opportunity to interact with the RHM–LHM interface. In such cases, the multiple scattering interactions between the RHMss and the LHMss do not exist. In other words, the wave components associated with $|S_{22}| = |S_{11}| = 1$ will not interact with the cloaking structure in the way predicted by equation (10); these wave components constitute backscattered components that reveal the cloaking structure’s presence. To clearly illustrate a scenario where such a

situation may arise, consider the situation where a light beam impinges upon the structure as shown in figure 5(b). If the shell is large, the light beam will simply be reflected by the shell and emerges out of port 1 by ray optics considerations. This corresponds to the case where $|S_{11}| = 1$ and clearly illustrates the failure of the cloaking structure. For now, we will only consider the simplest approach for maintaining cloaking integrity—by employing a sufficiently small shell (comparable to the wavelength) so that most of the incident wave components can interact with the RHM/LHM interface (i.e. $|S_{11}| \neq 1$), and thus equation (10) is valid.

3.2. Simulation of the RHM–PEC–LHM cloaking structure

In order to demonstrate the cloaking property of the proposed RHM–PEC–LHM structure, we performed a set of simulations using COMSOL Multiphysics [23]. The simulation setup is the same as in figure 3.

Figure 6 illustrates a number of scenarios where a TM wave impinges upon a conducting shell with and without the proposed cloaking structure. Displayed in each sub-figure is the real part of the magnetic-field phasor at 1 GHz so that the individual phase fronts are clearly visible. The direction of the power-flow lines (denoted as the black lines) is the direction of the Poynting vector and the line density is proportional to the magnitude of the magnetic field. The diagonal length of the conducting shell is 1.8λ . In figures 6(a)–(c), a plane wave at normal incidence is considered. In figures 6(d)–(g), an infinitesimally thin line source is used to generate a cylindrical wave. By comparing the scenarios where the cloaking structure is present (figures 6(a), (d) and (f)) to those where it is absent (figures 6(b), (e) and (g)), the ability of the cloaking structure to deflect the incident field minimally can be seen clearly. From figures 6(d) and (f), we can see that the cloaking structure also displaces the transmitted light field by an amount equal to its thickness, similar to the previous structure. Figure 6(c) is the plane-wave simulation of the present cloaking structure without the PEC caps.

In order to quantify the cloaking performance of the proposed structure, we calculate the far-field angular EM strength pattern and the far-field scattered EM strength pattern of an incident EM field from a line source on the structure, as shown in figure 7. In this set of simulations, the line source is located at a distance of 1.33λ from the center of the origin. In figure 7(a), the simulation is performed without any shell or cloaking structure; the plotted angular EM strength pattern is therefore unsurprisingly uniform. The second simulation (figure 7(b)) is performed with just the shell present. The interaction of the shell with the EM field results in a highly heterogeneous angular EM strength pattern and two strong forward scattering peaks can be found. The last simulation (figure 7(c)) is performed with the shell enveloped with the cloaking structure. We can see that the angular EM strength pattern approaches the uniformity of the first simulation. There are scattering peaks at angles close to 0° and 180° . This defect is due to the PEC boundaries on the proposed structure.

As described previously, the ratio of the shell size to the wavelength is an important point of cloaking quality consideration for this structure. Our next set of simulations aims to quantify the dependency for a range of sizes. We define the cloaking efficiency as the ratio of the total scattered power without the cloaking structure to the total scattered power with the cloaking structure. The illumination source used is a TM plane wave at normal incidence. The total scattered power is computed by taking the difference between the simulation solution and a simulation where nothing is present; a similar method was used in [24]. As shown in figure 8, the cloaking efficiency is high for small shells. The efficiency begins to drop rapidly beyond

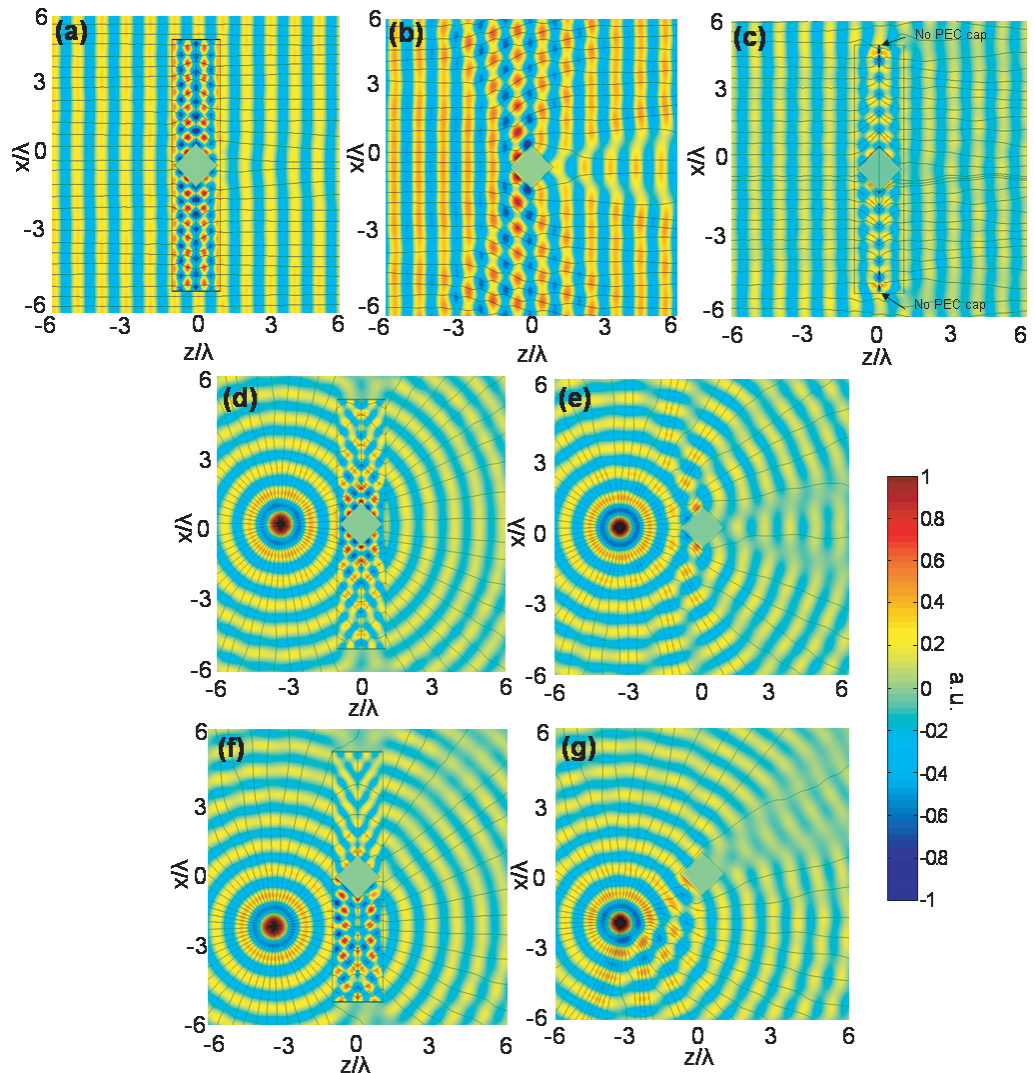


Figure 6. The simulated magnetic-field distribution and EM power-flow lines for the RHM-PEC-LHM structure. The computational domain is $3.6 \text{ m} \times 3.6 \text{ m}$ (12 wavelengths), where a 1 GHz transverse-electric TM polarized time-harmonic wave is incident upon a conducting shell with diagonal length 0.54 m (1.8 wavelengths). The width of the proposed cloaking structure in (a), (d) and (f) is 0.6 m (two wavelengths) and the height is 3 m (ten wavelengths). The permittivity and permeability of cloaking structure are $\varepsilon_1 = 2$, $\mu_1 = 1$, $\varepsilon'_1 = -2 + 0.01i$, $\mu'_1 = -1 + 0.01i$, $\varepsilon_0 = \varepsilon'_0 = \mu_0 = \mu'_0 = 1$. As a comparison, (b), (e) and (g) are the cases without the proposed cloaking structure. Figure 6(c) is the simulation of the proposed cloaking structure without PEC caps. For all the simulations, we use a perfect match layer (PML) in the outer boundaries to absorb the EM wave.

a shell size greater than 2λ , eventually tapering to unity (no cloaking activity) for the larger shells. We also note that, for the configuration of figures 6(a) and (c), the cloaking efficiency drops from 10.2 to 2.3 when the PEC caps are removed.

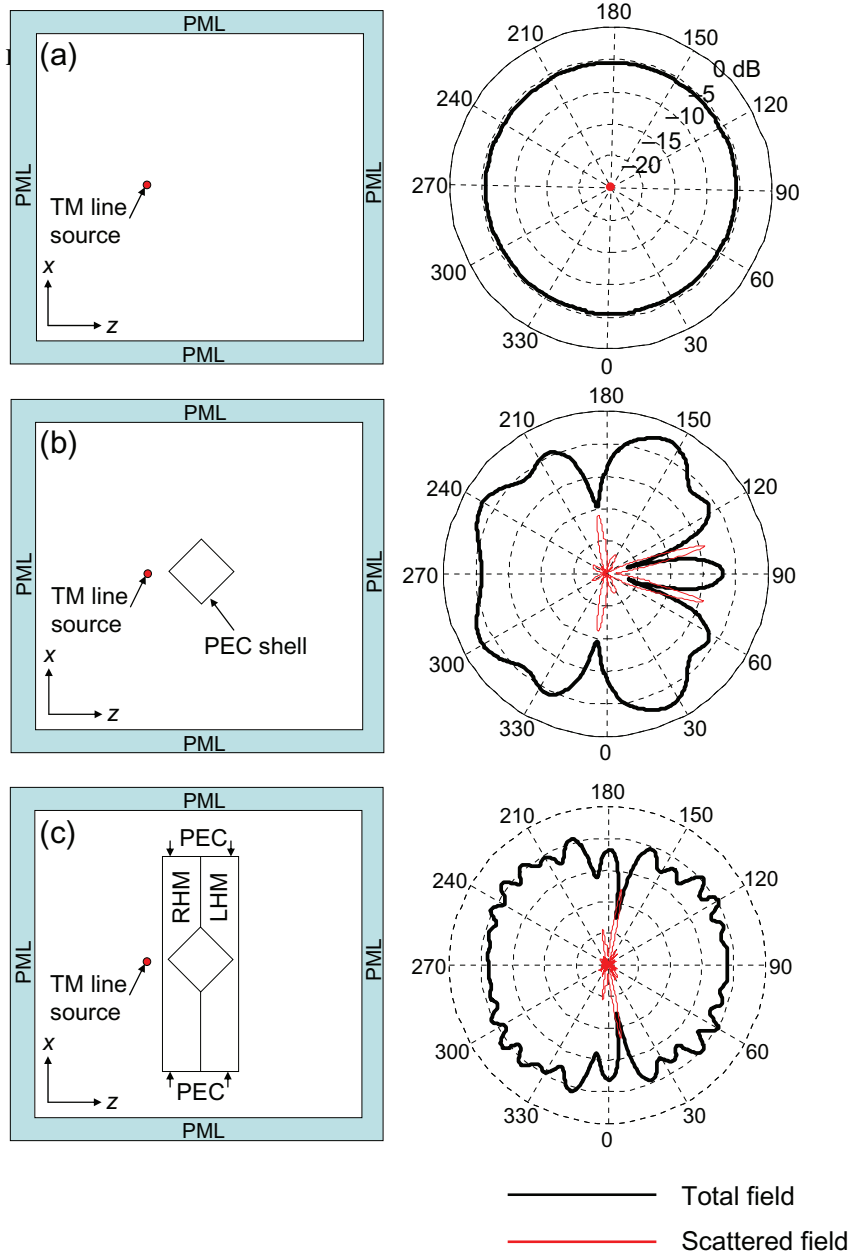


Figure 7. Study of the far-field patterns associated with a line source interacting with the proposed cloaking structure. (a) Line source only. The far-field angular pattern is uniform. (b) Line source and an uncloaked shell. The far-field angular pattern is highly non-isotropic because the shell scatters the incident light non-uniformly. (c) Line source and the proposed cloaking structure. The far-field angular pattern is more uniform. This indicates that the proposed structure has mitigated the scattering effect of the shell to some extent. (A loss term of $0.01i$ was imposed on the LHM to prevent the infinite resonance of the EM field at the interfaces.)

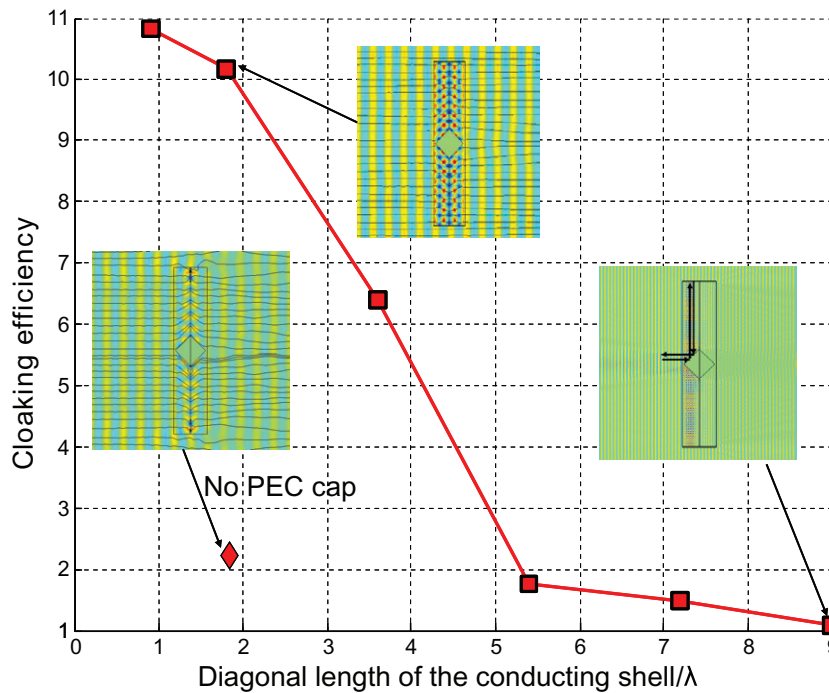


Figure 8. The size effect of the proposed cloaking structure. The cloaking efficiency here is defined as the ratio of the total scattered energy without the cloaking structure to the total scattered energy with the cloaking structure.

From the analysis of the simulations above, we see that the proposed RHM–PEC–LHM cloaking structure deviates from a Pendry’s cloak in the following aspects. Firstly, when the size of the conducting shell is very large compared to the wavelength, some wave components will be totally reflected back by the shell and they cannot be recovered on the other side of the structure. Secondly, the proposed structure fails to cloak when the EM field is incident at angles close to 0° and 180° —the presence of the perfectly conducting caps on the top and bottom of the structure interacts undesirably with such an EM field. Thirdly, the waves transmitted through the proposed structure have no phase retardation, and thus the outside observer will see a shifted image. In effect, the proposed cloaking structure will appear like a transparent but optically dense block to the observer. The second and third points of consideration are similar to points discussed for the first structure presented in this paper.

Of these limitations, the first is perhaps the most restrictive as it prevents effective cloaking of large objects. The small object restriction stems from our need to prevent $|S_{22}| = |S_{11}| = 1$ from occurring for a significant proportion of the light field components. There are several other strategies that may potentially be employed to prevent this condition from occurring. For example, we may consider seeding the RHMss and LHMss with dielectric scatterers as a way to scatter and diffuse light so that $|S_{22}| = |S_{11}| = 1$ does not occur for any incident EM field component. Another possible strategy is to design the shell appropriately (by customizing its shape, texturing its surface, etc) so that it never fully reflects any incident EM field component and instead always deflects some amount of the field towards the RHM–LHM interface (thus ensuring $|S_{22}| = |S_{11}| \neq 1$ is always true).

4. Conclusion

To conclude, two cloaking structures, which are inspired by the distortion–correction effect of PCMs, are proposed in this paper. The physical insight of the structure can be explained by the equivalency between the PCM and the RHM–LHM interface for propagative wave components. These proposed cloaking structures, in their current forms, are limited in their capability compared to Pendry’s cloak. However, we believe this alternate way of formulating cloaking structures is worth further examination as it may potentially lead to simpler cloaking structure formats for certain cloaking applications.

Acknowledgment

This work was supported by NSF career award BES-0547657.

References

- [1] Zel’dovich B Ya, Pilipetskii R F and Shkunov V V 1985 *Principles of Phase Conjugation* (Berlin: Springer)
- [2] Fisher R A 1983 *Optical Phase Conjugation* (New York: Academic)
- [3] Mittra R and Habashy T M 1984 *J. Opt. Soc. Am. A* **1** 1103
- [4] Agarwal G S, Friberg A T and Wolf E 1983 *J. Opt. Soc. Am.* **73** 529
- [5] Yaqoob Z, Psaltis D, Feld M S and Yang C 2008 *Nat. Photonics* **2** 110
- [6] Bozhevolnyi S I, Keller O and Smolyaninov I I 1994 *Opt. Lett.* **19** 1601
- [7] Bozhevolnyi S I, Keller O and Smolyaninov I I 1995 *Opt. Commun.* **115** 115
- [8] Mathey P, Odoulov S and Rytz D 2002 *Phys. Rev. Lett.* **89** 053901
- [9] Iizuka K 2002 *Elements of Photonics* (New York: Wiley-IEEE)
- [10] Zheng G A, Ran L X and Yang C H 2007 *Opt. Express* **15** 13877
- [11] Pendry J B, Schurig D and Smith D R 2006 *Science* **312** 1780
- [12] Leonhardt U 2006 *Science* **312** 1777
- [13] Leonhardt U 2006 *New J. Phys.* **8** 118
- [14] Schurig D, Mock J J, Justice B J, Cummer S A, Pendry J B, Starr A F and Smith D R 2006 *Science* **314** 977
- [15] Chen H, Wu B-I, Zhang B and Kong J A 2007 *Phys. Rev. Lett.* **99** 063903
- [16] Ruan Z, Yan M, Neff C W and Qiu M 2007 *Phys. Rev. Lett.* **99** 113903
- [17] Yan M, Ruan Z and Qiu M 2007 *Phys. Rev. Lett.* **99** 233901
- [18] Alu A and Engheta N 2005 *Phys. Rev. E* **72** 016623
- [19] Alu A and Engheta N 2008 *Phys. Rev. Lett.* **100** 113901
- [20] Carminati R, Saenz J J, Greffet J J and Nieto-Vesperinas M 2000 *Phys. Rev. A* **62** 012712
- [21] Pendry J B 2000 *Phys. Rev. Lett.* **85** 3966
- [22] Maslovski S and Tretyakov S 2003 *J. Appl. Phys.* **94** 4241
- [23] COMSOL INC 2007 *COMSOL Multiphysics 3.3* <http://www.comsol.com/>
- [24] Cummer S A, Popa B-I, Schurig D, Smith D R and Pendry J 2006 *Phys. Rev. E* **74** 036621